Slow Mixing of Glauber Dynamics for the Six-Vertex Model in the Ordered Phases

Matthew Fahrbach
School of Computer Science, Georgia Institute of Technology, Atlanta, Georgia, USA
matthew.fahrbach@gatech.edu

Dana Randall
School of Computer Science, Georgia Institute of Technology, Atlanta, Georgia, USA
randall@cc.gatech.edu

Abstract

The six-vertex model in statistical physics is a weighted generalization of the ice model on $\mathbb{Z}^2$ (i.e., Eulerian orientations) and the zero-temperature three-state Potts model (i.e., proper three-colorings). The phase diagram of the model represents its physical properties and suggests where local Markov chains will be efficient. In this paper, we analyze the mixing time of Glauber dynamics for the six-vertex model in the ordered phases. Specifically, we show that for all Boltzmann weights in the *ferroelectric phase*, there exist boundary conditions such that local Markov chains require exponential time to converge to equilibrium. This is the first rigorous result bounding the mixing time of Glauber dynamics in the ferroelectric phase. Our analysis demonstrates a fundamental connection between correlated random walks and the dynamics of intersecting lattice path models (or routings). We analyze the Glauber dynamics for the six-vertex model with free boundary conditions in the *antiferroelectric phase* and significantly extend the region for which local Markov chains are known to be slow mixing. This result relies on a Peierls argument and novel properties of weighted non-backtracking walks.

2012 ACM Subject Classification Theory of computation → Random walks and Markov chains

Keywords and phrases Correlated random walk, Markov chain Monte Carlo, Six-vertex model

Digital Object Identifier 10.4230/LIPIcs.APPROX-RANDOM.2019.37

Category RANDOM

Related Version A full version of the paper is available at `https://arxiv.org/abs/1904.01495`.

Funding *Matthew Fahrbach*: Supported in part by an NSF Graduate Research Fellowship under grant DGE-1650044.
Dana Randall: Supported in part by NSF grants CCF-1637031 and CCF-1733812.

1 Introduction

The *six-vertex model* was first introduced by Pauling in 1935 [33] to study the thermodynamics of crystalline solids with ferroelectric properties, and has since become one of the most compelling models in statistical mechanics. The prototypical instance of the model is the hydrogen-bonding pattern of two-dimensional ice – when water freezes, each oxygen atom must be surrounded by four hydrogen atoms such that two of the hydrogen atoms bond covalently with the oxygen atom and two are farther away. The state space of the six-vertex model consists of orientations of the edges in a finite region of the Cartesian lattice where every internal vertex has two incoming edges and two outgoing edges, also represented as Eulerian orientations of the underlying lattice graph. The model is most often studied on the $n \times n$ square lattice $\Lambda_n \subseteq \mathbb{Z}^2$ with $4n$ additional edges so that each internal vertex has degree 4. There are six possible edge orientations incident to a vertex (see Figure 1).

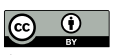

Approximation, Randomization, and Combinatorial Optimization. Algorithms and Techniques (APPROX/RANDOM 2019).
Editors: Dimitris Achlioptas and László A. Végh; Article No. 37; pp. 37:1–37:20

Leibniz International Proceedings in Informatics
Schloss Dagstuhl – Leibniz-Zentrum für Informatik, Dagstuhl Publishing, Germany

We assign Boltzmann weights $w_1, w_2, w_3, w_4, w_5, w_6 \in \mathbb{R}_{>0}$ to the six vertex types and define the partition function as $Z = \sum_{x \in \Omega} \prod_{i=1}^{6} w_i^{n_i(x)}$, where Ω is the set of Eulerian orientations of Λ_n and $n_i(x)$ is the number of type-i vertices in the configuration x.

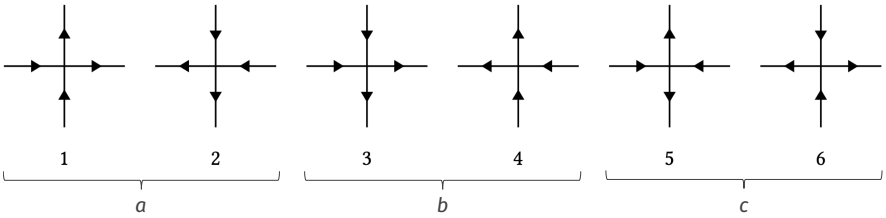

Figure 1 The valid edge orientations for internal vertices in the six-vertex model.

In 1967, Lieb discovered exact solutions to the six-vertex model with periodic boundary conditions for three different parameter regimes [25, 26, 27]. In particular, he famously showed that if all six vertex weights are $w_i = 1$, the energy per vertex is $\lim_{n\to\infty} Z^{1/n^2} = (4/3)^{3/2} = 1.5396007...$ (known as Lieb's square ice constant). His results were immediately generalized to allow for all parameter settings and external electric fields [38, 40]. An equivalence between periodic and free boundary conditions in the limit was established soon after [7], and since then the primary object of study has been the six-vertex model subject to *domain wall boundary conditions*, where the lower and upper boundary edges point into the square and the left and right boundary edges point outwards [20, 22, 6, 3, 4, 5]. There have been several surprisingly profound connections to enumerative combinatorics in this line of work. For instance, Zeilberger gave a sophisticated computer-assisted proof of the *alternating sign matrix conjecture* in 1995 [41]. A year later, Kuperberg [23] produced an elegant and significantly shorter proof using analysis of the partition function of the six-vertex model with domain wall boundary conditions. Other connections of the model to combinatorics and probability include tilings of the Aztec diamond and the arctic circle theorem [11, 14], sampling lozenge tilings [29, 39, 2], and enumerating 3-colorings of lattice graphs [36, 10].

While there has been extraordinary progress in understanding properties of the six-vertex model with periodic or domain wall boundary conditions, remarkably less is known when the model is subject to arbitrary boundary conditions. Sampling configurations using Markov chain Monte Carlo (MCMC) algorithms has been one of the primary means for discovering more general mathematical and physical properties of the six-vertex model [1, 31, 30, 21], and empirically the model is very sensitive to boundary conditions. Numerical studies have often observed slow convergence of local MCMC algorithms under certain parameter settings. For example, according to [30], "it must be stressed that the Metropolis algorithm might be impractical in the antiferromagnetic phase, where the system may be unable to thermalize." However, there are very few rigorous results for natural Markov chains and the computational complexity of sampling from the Boltzmann distribution for various weights and boundary conditions. This motivates our study of Glauber dynamics, the most widely used MCMC sampling algorithm, for the six-vertex model in the *ferroelectric* and *antiferroelectric phases*.

At first glance, there are six degrees of freedom in the model. However, this conveniently reduces to a two-parameter family due to invariants and standard physical assumptions that relate pairs of vertex types. To see this, it is useful to map configurations of the six-vertex model to sets of intersecting lattice paths by erasing all of the edges that are directed south or west and keeping the others [29]. Using this "routing interpretation," it is simple to see that the number of type-5 and type-6 vertices must closely correlated. In addition to revealing invariants, the lattice path representation of configurations turns out to be exceptionally

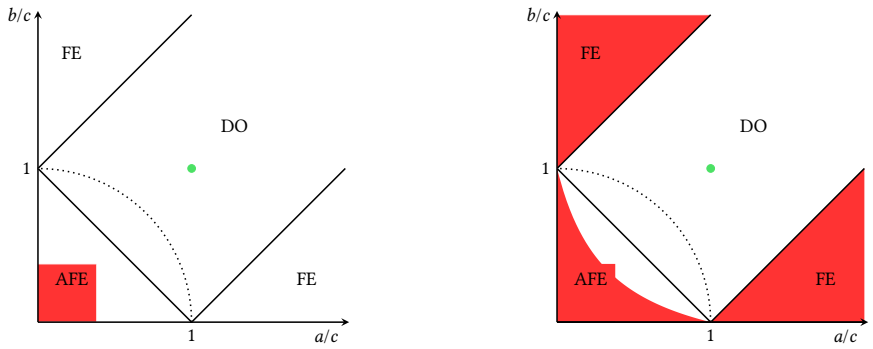

(a) (b)

Figure 2 Phase diagram of the six-vertex model with (a) previously known and (b) our current slowly mixing regions colored in red. Glauber dynamics is conjectured to be rapidly mixing for the entire disordered phase but has only been shown for the uniform distribution indicated by the green point $(1, 1)$ in both figures.

useful for analyzing Glauber dynamics. Moreover, the total weight of a configuration should remain unchanged if all the edge directions are reversed in the absence of an external electric field, so we let $w_1 = w_2 = a$, $w_3 = w_4 = b$, and $w_5 = w_6 = c$. This complementary invariance is known as the *zero field assumption*, and it is often convenient to exploit the conservation laws of the model [4] to reparameterize the system so that $w_1 = a^2$ and $w_2 = 1$. This allows us to ignore empty sites and focus solely on weighted lattice paths. Furthermore, since our goal is to sample configurations from the Boltzmann distribution, we can normalize the partition function by a factor of c^{-n^2} and consider the weights $(a/c, b/c, 1)$ instead of (a, b, c). We collectively refer to these properties as the invariance of the Gibbs measure for the six-vertex model.

The phase diagram of the six-vertex model represents physical properties of the system and is partitioned into three regions: the *disordered* (DO) phase, the *ferroelectric* (FE) phase, and the *antiferroelectric* (AFE) phase. To establish these regions, we consider the parameter

$$\Delta = \frac{a^2 + b^2 - c^2}{2ab}.$$

The disordered phase is the set of parameters $(a, b, c) \in \mathbb{R}^3_{>0}$ that satisfy $|\Delta| < 1$, and Glauber dynamics is expected to be rapidly mixing in this region because there are no long-range correlations in the system. The ferroelectric phase is defined by $\Delta > 1$, or equivalently when $a > b + c$ or $b > a + c$. We show in this paper that Glauber dynamics can be slow mixing at any point in this region (Figure 2b). The antiferroelectric phase is defined by $\Delta < -1$, or equivalently when $a + b < c$, and our second result significantly extends the antiferroelectric subregion for which Glauber dynamics is known to be slow mixing. The phase diagram is symmetric over the main positive diagonal, which follows from the fact that a and b are interchangeable under the automorphism that rotates each of the six vertex types by ninety degrees clockwise. Under the zero field assumption, this is equivalent to rotating the entire model, so we can assume without loss of generality that if a mixing result holds for one point in the phase diagram, it also holds at the point reflected over the main diagonal.

Cai, Liu, and Lu [9] recently provided strong evidence supporting conjectures about the approximability of the six-vertex model. In particular, they designed a *fully randomized approximation scheme* (FPRAS) for a subregion of the disordered phase that works for all 4-regular graphs via the winding framework for Holant problems [32, 19]. They also showed

that there cannot exist an FPRAS for 4-regular graphs in the ferroelectric or antiferroelectric phases unless $\mathbf{RP} = \mathbf{NP}$. We note that their hardness result uses nonplanar gadgets and the larger class of 4-regular graphs, so it does not reveal anything about the complexity of Glauber dynamics for the six-vertex model on regions of $\mathbb{Z}^2$. A dichotomy theorem for the (exact) computability of the partition function of the six-vertex model on 4-regular graphs was also recently proven in [8]. As for the positive results, Luby, Randall, and Sinclair [29] proved rapid mixing of a Markov chain that leads to a fully polynomial almost uniform sampler for Eulerian orientations on any region of the Cartesian lattice with fixed boundaries (i.e., the unweighted case when $a/c = b/c = 1$). Randall and Tetali [36] then used a comparison technique to argue that Glauber dynamics for Eulerian orientations on lattice graphs is rapidly mixing by relating this Markov chain to the Luby-Randall-Sinclair chain. Goldberg, Martin, and Paterson [16] extended their approach to show that Glauber dynamics is rapidly mixing on rectangular lattice regions with free boundary conditions.

Liu [28] recently gave the first rigorous result that Glauber dynamics is slowly mixing in a subregion of an ordered phase by showing that local Markov chains require exponential time to converge in the antiferroelectric subregion defined by $\max(a, b) < c/\mu$, where $\mu = 2.6381585...$ is the connective constant for self-avoiding walks on the square lattice (Figure 2a). He also showed that the directed loop algorithm mixes slowly in the same antiferroelectric subregion and for all of the ferroelectric region, but this has no bearing on the efficiency of Glauber dynamics in the ferroelectric region. We note that the partition function is exactly computable for all boundary conditions at the free-fermion point when $\Delta = 0$, or equivalently $a^2 + b^2 = c^2$, via a reduction to domino tilings and a Pfaffian computation [14]. There is strong evidence that exact counting is unlikely anywhere else for arbitrary boundary conditions [8].

1.1 Main Results

In this paper we show that there exist boundary conditions for which Glauber dynamics mixes slowly for the six-vertex model in the ferroelectric and antiferroelectric phases. We start by proving that there are boundary conditions that cause Glauber dynamics to be slow for all Boltzmann weights that lie in the ferroelectric region of the phase diagram, where the mixing time is exponential in the number of vertices in the lattice. This is the first rigorous result for the mixing time of Glauber dynamics in the ferroelectric phase and it gives a complete characterization.

▶ **Theorem 1** (Ferroelectric phase). *For any $(a, b, c) \in \mathbb{R}^3_{>0}$ such that $a > b + c$ or $b > a + c$, there exist boundary conditions for which Glauber dynamics mixes exponentially slowly on Λ_n.*

We note that our approach naturally breaks down at the critical line in a way that reveals a trade-off between the energy and entropy of the system. Additionally, our analysis suggests an underlying combinatorial interpretation for the phase transition between the ferroelectric and disordered phases in terms of the adherence strength of intersecting lattice paths and the momentum parameter of correlated random walks.

Our second mixing result builds on the topological obstruction framework developed in [35] to show that Glauber dynamics with free boundary conditions mixes slowly in most of the antiferroelectric region. Specifically, we generalize the recent antiferroelectric mixing result in [28] with a Peierls argument that uses multivariate generating functions for weighted non-backtracking walks instead of the connectivity constant for (unweighted) self-avoiding walks to better account for the discrepancies in Boltzmann weights.

▶ **Theorem 2** (Antiferroelectric phase). *For any $(a, b, c) \in \mathbb{R}^3_{>0}$ such that $ac + bc + 3ab < c^2$, Glauber dynamics mixes exponentially slowly on Λ_n with free boundary conditions.*

We illustrate the new regions for which Glauber dynamics can be slowly mixing in Figure 2. Observe that our antiferroelectric subregion significantly extends Liu's and pushes towards the conjectured threshold.

1.2 Techniques

We take significantly different approaches for our analysis of the ferroelectric and antiferroelectric phases. In the ferroelectric phase, where $a > b + c$ and type-a vertices are preferred to type-b and type-c vertices, we construct boundary conditions that induce polynomially-many paths separated by a critical distance that allows all of the paths to (1) behave independently and (2) simultaneously intersect with their neighbors maximally. (This analysis also covers the case $b > a + c$ by a standard invariant that shows symmetry in the phase diagram over the line $y = x$.) From here, we analyze the dynamics of a single path in isolation as an escape probability, which eventually allows us to bound the conductance of the Markov chain. The dynamics of a single lattice path are equivalent to a those of a *correlated random walk*. In Appendix A we present a new tail inequality for correlated random walks that accurately bounds the probability of large deviations from the starting position. We note that decomposing the dynamics of lattice models into one-dimensional random walks has recently been shown to achieve nearly tight bounds for escape probabilities in a different setting [12].

One of the key technical contributions in this paper is our analysis of the tail behavior of correlated random walks in Appendix A. While there is a simple combinatorial expression for the position of a correlated random walk written as a sum of marginals, it is not immediately useful for bounding the displacement from the origin. To achieve an exponentially small tail bound for these walks, we first construct a smooth function that tightly upper bounds the marginals and then optimize this function to analyze the asymptotics of the log of the maximum marginal. Once we obtain an asymptotic equality for the maximum marginal, we can upper bound the deviation of a correlated random walk, and hence the deviation of a lattice path in a configuration. Ultimately, this allows us to show that there exists a balanced cut in the state space that has an exponentially small escape probability, which implies that the Glauber dynamics are slowly mixing.

In the antiferroelectric phase, on the other hand, the Boltzmann weights satisfy $a + b < c$ so type-c vertices are preferred. It follows that there are two (arrow-reversal) symmetric ground states of maximum probability containing only type-c vertices. To move between configurations that agree predominantly with different ground states, the Markov chain must pass through configurations with a large number of type-a or type-b vertices. Using the idea of *fault lines* introduced in [35], we use self-avoiding walks to characterize such configurations and construct a cut set with exponentially small probability mass that separates the ground states. Liu [28] follows this Peierls argument approach and bounds the weight of the cut by separately considering the minimum energy gain of the corresponding inverse map and the number of preimages (i.e., the entropy). Instead, we directly bound the free energy (rather than as a product of the upper bounds for the energy and entropy terms) and are able to show slow mixing for a much larger region of the phase diagram. Our key observation for accurately bounding the free energy is that when a fault line changes direction, the vertices along it switch from type-a to type-b or vice versa. Therefore, we introduce the notion of *weighted non-backtracking walks* and solve their multivariate generating function by diagonalizing a system of linear recurrences to exactly account for disparities between the weights of a and b along fault lines.

2 Preliminaries

We start by reviewing some necessary background on Markov chains, Glauber dynamics, and correlated random walks.

2.1 Markov Chains and Mixing Times

Let $\mathcal{M}$ be an ergodic, reversible Markov chain with finite state space Ω, transition probability matrix P, and stationary distribution π. The t-step transition probability from states x to y is denoted as $P^t(x, y)$. The total variation distance between the probability distributions μ and ν on Ω is

$$\|\mu - \nu\|_{\text{TV}} = \frac{1}{2} \sum_{x \in \Omega} |\mu(x) - \nu(x)|.$$

The *mixing time* of $\mathcal{M}$ is $\tau(1/4) = \min\{t \in \mathbb{Z}_{\geq 0} : \max_{x \in \Omega} \|P^t(x, \cdot) - \pi\|_{\text{TV}} \leq 1/4\}$. We say that $\mathcal{M}$ is rapidly mixing if its mixing time is $O(\text{poly}(n))$, where n is the size of each configuration in the state space. Similarly, we say that $\mathcal{M}$ is slow mixing if its mixing time is $\Omega(\exp(n^c))$ for some constant $c > 0$.

The mixing time of a Markov chain is characterized by its *conductance* (up to polynomial factors). The conductance of a nonempty set $S \subseteq \Omega$ is

$$\Phi(S) = \frac{\sum_{x \in S, y \notin S} \pi(x) P(x, y)}{\pi(S)},$$

and the conductance of the Markov chain is $\Phi^* = \min_{S \subseteq \Omega : 0 < \pi(S) \leq 1/2} \Phi(S)$. It is often useful to view the conductance of a set as an escape probability – starting from stationarity and conditioned on being in S, the conductance $\Phi(S)$ is the probability that $\mathcal{M}$ leaves S in one step.

▶ **Theorem 3** ([24]). *For an ergodic, reversible Markov chain with conductance Φ^*, we have $\tau(1/4) \geq 1/(4\Phi^*)$.*

To show that a Markov chain is slow mixing, it suffices to show that the conductance is exponentially small.

In this paper we the study single-site *Glauber dynamics* for the six-vertex model. This Markov chain makes local moves by (1) choosing an internal cell of the lattice uniformly at random and (2) reversing the orientations of the edges that bound the chosen cell if they form a cycle. In the lattice path interpretation of the model, these dynamics correspond to the mountain-valley Markov chain that flips corners. Transitions between states are made according to the Metropolis-Hastings acceptance probability so that the Markov chain converges to the desired stationary distribution.

2.2 Correlated Random Walks

A key tool in our analysis for the ferroelectric phase are correlated random walks, which generalize simple symmetric random walks by accounting for momentum. A *one-dimensional correlated random walk* with momentum parameter $p \in [0, 1]$ starts at the origin and is defined as follows. Let X_1 be a uniform random variable with support $\{-1, 1\}$. For all subsequent steps $i \geq 2$, the direction of the process is correlated with the direction of the previous step and satisfies

$$X_{i+1} = \begin{cases} X_i & \text{with probability } p, \\ -X_i & \text{with probability } 1 - p. \end{cases}$$

We denote the position of the walk at time t by $S_t = \sum_{i=1}^{t} X_i$. It will often be useful to make the change of variables $p = \mu/(1+\mu)$ when analyzing the six-vertex model. In many cases this also leads to cleaner expressions. We use the following probability density function (PDF) for the position of a correlated random walk to develop a new tail inequality (Lemma 8) that holds for all values of p.

▶ **Lemma 4** ([18]). *For any $n \geq 1$ and $m \geq 0$, the PDF of a correlated random walk is*

$$\Pr(S_{2n} = 2m) = \begin{cases} \frac{1}{2}p^{2n-1} & \text{if } 2m = 2n, \\ \sum_{k=1}^{n-m} \binom{n+m-1}{k-1}\binom{n-m-1}{k-1}(1-p)^{2k-1}p^{2n-1-2k}\left(\frac{n(1-p)+k(2p-1)}{k}\right) & \text{if } 2m < 2n. \end{cases}$$

3 Slow Mixing in the Ferroelectric Phase

We start with the ferroelectric phase where $a > b+c$ or $b > a+c$, and we give a conductance-based argument to show that Glauber dynamics can be slowly mixing in the entire ferroelectric region. Specifically, we show that there exist boundary conditions that induce an exponentially small, asymmetric bottleneck in the state space, revealing a natural trade-off between the energy and entropy in the system. Viewing the six-vertex model in the intersecting lattice interpretation suggests how to plant polynomially-many paths in the grid that can (1) be analyzed independently, while (2) being capable of intersecting maximally. This path independence makes our analysis tractable and allows us to interpret the dynamics of a path as a correlated random walk, for which we develop an exponentially small tail bound in Appendix A. Since escape probabilities govern mixing times [34], we show how to relate the expected maximum deviation of a correlated walk to the conductance of the Markov chain to prove slow mixing. In addition to showing slow mixing up to the conjectured threshold, a surprising feature of our argument is that it potentially gives a combinatorial explanation for the phase transition from the ferroelectric to disordered phase. In particular, Lemma 9 demonstrates how the parameters of the model delicately balance the probability mass of the Markov chain.

Next, we exploit the invariance of the Gibbs measure and the lattice path interpretation of the six-vertex model to conveniently reparameterize the Boltzmann weights. Specifically, we let $w_1 = \lambda^2$ and $w_2 = 1$ so that we can ignore empty sites. Note that $a = \sqrt{w_1 w_2} = \lambda$. We also let $b = w_2 = w_3 = \mu$ and $c = w_5 = w_6 = 1$ so that the weight of a configuration only comes from straight segments and intersections of neighboring lattice paths.

3.1 Constructing the Boundary Conditions and Cut

We begin with a few colloquial definitions for lattice paths that allow us to easily construct the boundary conditions and make arguments about the conductance of the Markov chain. We call a $2n$-step, north-east lattice path γ starting from $(0,0)$ a *path of length* $2n$, and if the path ends at (n,n) we describe it as *tethered*. If $\gamma = ((0,0),(x_1,y_1),(x_2,y_2),\ldots,(x_{2n},y_{2n}))$, we define the *deviation* of γ to be $\max_{i=0..2n}\|(x_i,y_i) - (i/2,i/2)\|_1$. Geometrically, path deviation captures the (normalized) maximum perpendicular distance of the path to the line $y = x$. We refer to vertices (x_i,y_i) along the path as *corners* or *straights* depending on whether or not the path turned. If two paths intersect at a vertex we call this site a *cross*. Note that this classifies all vertex types in the six-vertex model.

We consider the following *independent paths boundary condition* for an $n \times n$ six-vertex model for the rest of the section. To construct this boundary condition, we consider its lattice path interpretation. First, place a tethered path γ_0 that enters $(0,0)$ horizontally and exits (n,n) horizontally. Next, place $2\ell = \lfloor n^{1/8} \rfloor$ translated tethered paths of varying

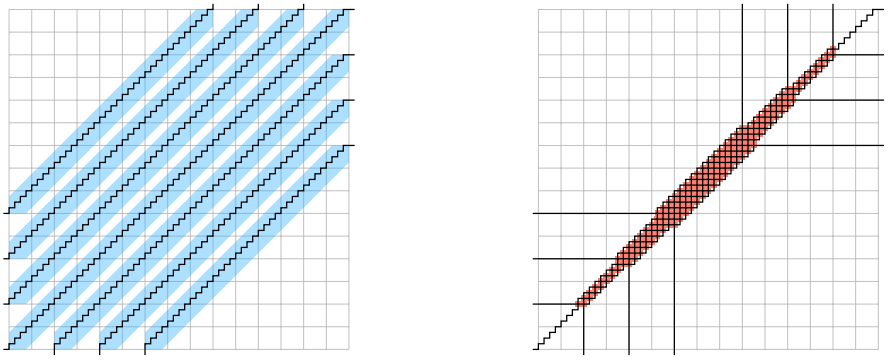

(a) (b)

Figure 3 Examples of states with the independent paths boundary condition: (a) is a state in S with the deviation bounds highlighted and (b) is the ground state in the ferroelectric phase.

length above and below the main diagonal, each separated from its neighbors by distance $d = \lfloor 32n^{3/4} \rfloor$. Specifically, the paths $\gamma_1, \gamma_2, \ldots, \gamma_\ell$ below the main diagonal begin at the vertices $(d, 0), (2d, 0), \ldots, (\ell d, 0)$ and end at the vertices $(n, n-d), (n, n-2d), \ldots, (n, n-\ell d)$, respectively. The paths $\gamma_{-1}, \gamma_{-2}, \ldots, \gamma_{-\ell}$ above the main diagonal begin at $(0, d), (0, 2d), \ldots, (0, \ell d)$ and end at $(n-d, n), (n-2d, n), \ldots, (n-\ell d, n)$. The deviation of a translated tethered path is the deviation of the same path starting at $(0, 0)$. To complete the boundary condition, we force the paths below the main diagonal to enter vertically and exit horizontally. Symmetrically, we force the paths above the main diagonal to enter horizontally and exit vertically. See Figure 3a for an illustration of the construction when all paths have small deviation.

Next, we construct an asymmetric cut in the state space induced by this boundary condition in terms of its internal lattice paths. In particular, we analyze a set S of configurations such that every path in a configuration has small deviation. Formally, we let

$$S \stackrel{\text{def}}{=} \left\{ x \in \Omega : \text{the deviation of each path in } x \text{ is less than } 8n^{3/4} \right\}.$$

Observe that by our choice of separation distance $d = \lfloor 32n^{3/4} \rfloor$ and the deviation limit for S, no paths in any configuration of S intersect. It follows that the partition function for S factors into a product of $2\ell + 1$ partition functions, one for each path with bounded deviation. This intuition is useful when analyzing the conductance $\Phi(S)$ as an escape probability from stationarity.

3.2 Lattice Paths as Correlated Random Walks

Now we consider weighting the internal paths according to the six-vertex model. The main result in this subsection is that random tethered paths are exponentially unlikely to deviate past $\omega(n^{1/2})$, even if drawn from a Boltzmann distribution that favors straights (Lemma 5). Let $\Gamma(\mu, n)$ denote the distribution over tethered paths of length $2n$ such that

$$\Pr(\gamma) \propto \mu^{(\#\text{ of straights in } \gamma)}.$$

▶ **Lemma 5.** *Let $\mu, \varepsilon > 0$ and $m = o(n)$. For n sufficiently large and $\gamma \sim \Gamma(\mu, n)$, we have* $\Pr(\gamma \text{ deviates by at least } 2m) \leq e^{-(1-\varepsilon)\frac{m^2}{\mu n}}$.

We defer the proof of Lemma 5 to the full version of the paper [13]. Instead, we sketch its key ideas to demonstrate the connection between biased tethered paths and correlated random walks, and to show how the supporting lemmas interact.

First, observe that there is a natural measure-preserving bijection between biased tethered paths of length $2n$ and correlated random walks of length $2n$ that return to the origin. Concretely, for a correlated random walk $(S_0, S_1, \dots, S_{2n})$ parameterized by $p = \mu/(1+\mu)$,

$$\Pr(\gamma \text{ deviates by at least } 2m) = \Pr\Big(\max_{i=0..2n} |S_i| \geq 2m \;\Big|\; S_{2n} = 0\Big). \tag{1}$$

Now we present an asymptotic equality that generalizes the return probability of simple symmetric random walks. This allows us to relax the condition in (1) that a correlated random walk returns to the origin, and instead we bound $\Pr(\max_{i=0..2n} |S_i| \geq 2m)$ at the expense of an additional polynomial factor.

▶ **Lemma 6** ([15]). *For any constant $\mu > 0$, the return probability of a correlated random walk is $\Pr(S_{2n} = 0) \sim 1/\sqrt{\mu\pi n}$.*

Another result needed to prove Lemma 5 is that the PDF for correlated random walks is unimodal.

▶ **Lemma 7.** *For any momentum parameter $p \in (0,1)$ and n sufficiently large, the probability of the position of a correlated random walk is unimodal. Concretely, for $m \in \{0, 1, \dots, n-1\}$, we have $\Pr(S_{2n} = 2m) \geq \Pr(S_{2n} = 2(m+1))$.*

Last, we give an upper bound for the position of a correlated random walk. We fully develop this inequality in Appendix A by analyzing the asymptotic behavior of the PDF in Lemma 4. Observe that Lemma 8 demonstrates exactly how the tail behavior of simple symmetric random walks generalizes to correlated random walks as a function of μ.

▶ **Lemma 8.** *Let $\mu, \varepsilon > 0$ and $m = o(n)$. For n sufficiently large, a correlated random walk satisfies $\Pr(S_{2n} = 2m) \leq e^{-(1-\varepsilon)\frac{m^2}{\mu n}}$.*

To complete the proof sketch of Lemma 5, we start by using Lemma 6 to relax the conditional probability. It follows from Lemma 7 and union bounds that

$$\Pr\Big(\max_{i=0..2n} |S_i| \geq 2m \;\Big|\; S_{2n} = 0\Big) \leq 2\sqrt{\mu\pi n} \cdot 2n^2 \cdot \Pr(S_{2n} = 2m). \tag{2}$$

Applying Lemma 8 to (2) with a smaller error completes the proof. See [13] for more details.

3.3 Bounding the Conductance and Mixing Time

Next, we bound the conductance of the Markov chain by viewing $\Phi(S)$ as an escape probability. We start by claiming that $\pi(S) \leq 1/2$ (as required by the definition of conductance) if and only if the parameters are in the ferroelectric phase. Due to space constraints, we also defer the proof of Lemma 9 to [13]. Then we use the correspondence between tethered paths and correlated random walks (Section 3.2) to prove that $\Phi(S)$ is exponentially small.

▶ **Lemma 9.** *Let $\mu > 0$ and $\lambda > 1 + \mu$ be constants. For n sufficiently large, $\pi(S) \leq 1/2$.*

Our analysis of the escape probability from S critically relies on the fact that paths in any state $x \in S$ are non-intersecting. Combinatorially, we exploit the factorization of the generating function for states in S as a product of $2\ell+1$ independent path generating functions.

▶ **Lemma 10.** *Let $\mu, \varepsilon > 0$ be constants. For n sufficiently large, $\Phi(S) \le e^{-(1-\varepsilon)\mu^{-1}n^{1/2}}$.*

Proof. The conductance $\Phi(S)$ can be understood as the following escape probability. Sample a state $x \in S$ from the stationary distribution π conditioned on $x \in S$, and run the Markov chain from x for one step to get a neighboring state y. The definition of conductance implies that $\Phi(S)$ is the probability that $y \notin S$. Using this interpretation, we can upper bound $\Phi(S)$ by the probability mass of states that are near the boundary of S in the state space, since the process must escape in one step. Therefore, it follows from the independent paths boundary condition and the definition of S that

$$\Phi(S) \le \Pr\Big(\text{there exists a path in } x \text{ deviating by at least } 4n^{3/4} \;\Big|\; x \in S\Big).$$

Next, we use a union bound over the $2\ell+1$ different paths in a configuration and consider the event that a particular path γ_k deviates by at least $4n^{3/4}$. Because all of the paths in S are independent, we only need to consider the behavior of γ_k in isolation. This allows us to rephrase the conditional event. Relaxing the conditional probability of each term in the sum gives

$$\begin{aligned}
\Phi(S) &\le \sum_{k=-\ell}^{\ell} \Pr\Big(\gamma_k \text{ deviates by at least } 4n^{3/4} \;\Big|\; x \in S\Big) \\
&= \sum_{k=-\ell}^{\ell} \Pr\Big(\gamma_k \text{ deviates by at least } 4n^{3/4} \;\Big|\; \gamma_k \text{ deviates by less than } 8n^{3/4}\Big) \\
&\le \sum_{k=-\ell}^{\ell} \frac{\Pr\big(\gamma_k \text{ deviates by at least } 4n^{3/4}\big)}{1 - \Pr\big(\gamma_k \text{ deviates by at least } 8n^{3/4}\big)}.
\end{aligned}$$

For large enough n, the length of every path γ_k is in the range $[n, 2n]$ since we eventually have $n - \ell d \ge n/2$. Therefore, we can apply Lemma 5 with the error $\varepsilon/2$ to each term and use the universal upper bound

$$\frac{\Pr\big(\gamma_k \text{ deviates by at least } 4n^{3/4}\big)}{1 - \Pr\big(\gamma_k \text{ deviates by at least } 8n^{3/4}\big)} \le \frac{e^{-\left(1-\frac{\varepsilon}{2}\right)\frac{16n^{3/2}}{\mu n}}}{1 - e^{-\left(1-\frac{\varepsilon}{2}\right)\frac{64n^{3/2}}{\mu n}}} \le 2e^{-\left(1-\frac{\varepsilon}{2}\right)\frac{16n^{3/2}}{\mu n}}.$$

It follows from the union bound and previous inequality that the conductance $\Phi(S)$ is bounded by

$$\Phi(S) \le (2\ell+1) \cdot 2e^{-\left(1-\frac{\varepsilon}{2}\right)\frac{16n^{3/2}}{\mu n}} \le e^{-(1-\varepsilon)\mu^{-1}n^{1/2}},$$

which completes the proof. ◀

▶ **Theorem 11.** *Let $\mu, \varepsilon > 0$ and $\lambda > 1 + \mu$. For n sufficiently large, $\tau(1/4) \ge e^{(1-\varepsilon)\mu^{-1}n^{1/2}}$.*

Proof. Since $\pi(S) \le 1/2$ by Lemma 9, we have $\Phi^* \le \Phi(S)$. The proof follows from Theorem 3 and the conductance bound in Lemma 10 with a smaller error $\varepsilon/2$. ◀

Last, we restate our main theorem and use Theorem 11 to show that Glauber dynamics for the six-vertex model can be slow mixing for all parameters in the ferroelectric phase.

▶ **Theorem 1** (Ferroelectric phase). *For any $(a, b, c) \in \mathbb{R}^3_{>0}$ such that $a > b + c$ or $b > a + c$, there exist boundary conditions for which Glauber dynamics mixes exponentially slowly on Λ_n.*

Proof. Without loss of generality, we reparameterized the model so that $a = \lambda$, $b = \mu$, and $c = 1$. Therefore, Glauber dynamics with the independent paths boundary condition is slow mixing if $a > b + c$ by Theorem 11. Since the rotational invariance of the six-vertex model implies that a and b are interchangeable parameters, this mixing time result also holds in the case $b > a + c$. ◀

4 Slow Mixing in the Antiferroelectric Phase

Now we consider the mixing time of Glauber dynamics in the antiferroelectric phase, where $c > a + b$ and corners (type-c vertices) are preferred. The main insight behind our slow mixing proof is that when c is sufficiently large, the six-vertex model can behave like the low-temperature hardcore model on $\mathbb{Z}^2$ where configurations predominantly agree with one of two ground states. Liu recently formalized this argument in [28] and showed that Glauber dynamics for the six-vertex model with free boundary conditions requires exponential time when $\max(a, b) < \mu c$, where $\mu \leq 2.639$ is the connective constant of self-avoiding walks on the square lattice [17]. His proof uses a Peierls argument based on topological obstructions introduced by Randall [35] in the context of independent sets. We extend Liu's result to the region depicted in Figure 2b by computing a closed-form multivariate generating function that upper bounds the number of self-avoiding walks and accounts for disparities in their Boltzmann weights induced by the parameters of the six-vertex model.

4.1 Topological Obstruction Framework

We start with a recap of the definitions and framework laid out in [28]. There are two ground states in the antiferroelectric phase such that every interior vertex is a corner: x_{R} (Figure 4a) and x_{G} (Figure 4b). These configurations are edge reversals of each other, so for any $x \in \Omega$ we can color its edges *red* if they are oriented as in x_{R} or *green* if they are oriented as in x_{G}. See Figure 4c for an example. It follows from case analysis of the six vertex types (Figure 1) that the number of red edges incident to any internal vertex is even, and if there are only two red edges then they must be rotationally adjacent to each other. The same property holds for green edges by symmetry. Note that the four edges bounding a cell of the lattice are monochromatic if and only if they are oriented cyclically, and thus reversible by Glauber dynamics. We say that a simple path from a horizontal edge on the left boundary of Λ_n to a horizontal edge on the right boundary is a *red horizontal bridge* if it contains only red edges. We define green horizontal bridges and monochromatic vertical bridges similarly. A configuration has a *red cross* if it contains both a red horizontal bridge and a red vertical bridge, and we define a *green cross* likewise. Let $C_{\mathrm{R}} \subseteq \Omega$ be the set of all states with a red cross, and let $C_{\mathrm{G}} \subseteq \Omega$ be the set of all states with a green cross. We have $C_{\mathrm{R}} \cap C_{\mathrm{G}} = \emptyset$ by Lemma 12.

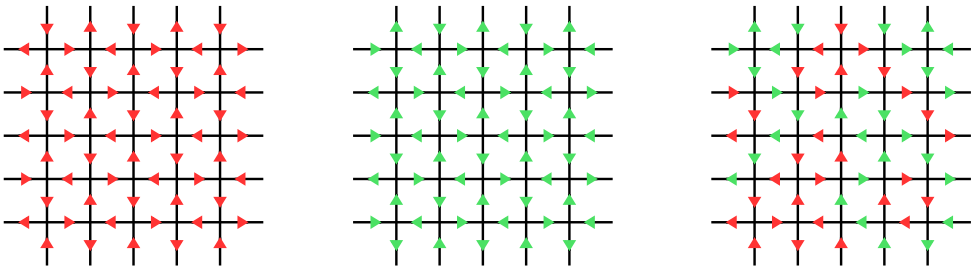

Figure 4 Edge colorings of (a) the red ground state x_{R}, (b) the green ground state x_{G}, and (c) an example configuration with free boundary conditions that does not have a monochromatic cross.

Next, we define the dual lattice L_n to describe configurations in $\Omega \setminus (C_{\mathrm{R}} \cup C_{\mathrm{G}})$. The vertices of L_n are the centers of the cells in Λ_n, including the cells on the boundary that are partially enclosed, and we connect dual vertices by an edge if their corresponding cells are diagonally adjacent. Note that L_n is a union of two disjoint graphs (Figure 5a). For any state $x \in \Omega$ there is a corresponding dual subgraph L_x defined as follows: for each interior vertex v in Λ_n, if v is incident to two red edges and two green edges, then L_x contains the dual edge passing through v that separates the two red edges from the two green edges. This construction is well-defined because the red edges are rotationally adjacent. See Figure 5b for an example. For any $x \in \Omega$, we say that x has a *horizontal fault line* if L_x contains a simple path from a left dual boundary vertex to a right dual boundary vertex. We define horizontal fault lines similarly and let $C_{\mathrm{FL}} \subseteq \Omega$ be the set of all states containing a horizontal or vertical fault line. Observe that fault lines completely separate red and green edges, and hence are topological obstructions that prohibit monochromatic bridges.

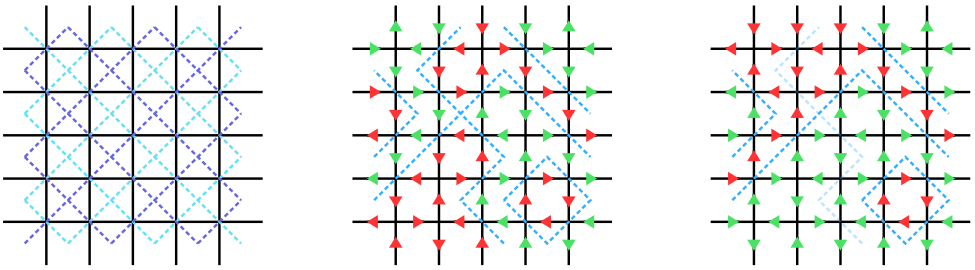

Figure 5 Illustrations of (a) the dual lattice L_n as a union of disjoint cyan and purple subgraphs, (b) an example configuration overlaid with its dual graph, and (c) the example under the injective fault line map.

Last, we extend the notion of fault lines to *almost fault lines*. We say that $x \in \Omega$ has a horizontal almost fault line if there is a simple path in L_n connecting a left dual boundary vertex to a right dual boundary vertex such that all edges except for one are in L_x. We define vertical almost fault lines similarly and let the set $C_{\mathrm{AFL}} \subseteq \Omega$ denote all states containing an almost fault line. Finally, let $\partial C_{\mathrm{R}} \subseteq \Omega$ denote the set of states not in C_{R} that one move away from C_{R} in the state space according to the Glauber dynamics.

▶ **Lemma 12** ([28]). *We can partition the state space into* $\Omega = C_{\mathrm{R}} \cup C_{\mathrm{FL}} \cup C_{\mathrm{G}}$. *Furthermore, we have* $\partial C_{\mathrm{R}} \subseteq C_{\mathrm{FL}} \cup C_{\mathrm{AFL}}$.

4.2 Weighted Non-Backtracking Walks and a Peierls Argument

In this subsection we show that $\pi(C_{\mathrm{FL}} \cup C_{\mathrm{AFL}})$ is an exponentially small bottleneck in the state space Ω. The analysis relies on Lemma 12 and a new multivariate upper bound for weighted self-avoiding walks (Lemma 13). Our key observation is that when a fault line changes direction, the vertices in its path change from type-a to type-b or vice versa. Therefore, our goal in this subsection is to generalize the trivial 3^{n-1} upper bound for the number of self-avoiding walks by accounting for their changes in direction in aggregate. We achieve this by using generating functions to solve a system of linear recurrence relations.

We start by encoding *non-backtracking walks* that start from the origin and take their first step northward using the characters in $\{\mathsf{S}, \mathsf{L}, \mathsf{R}\}$, representing straight, left, and right steps. For example, the walk SLRSSL corresponds uniquely to the sequence

$((0,0),(0,1),(-1,1),(-1,2),(-1,3),(-1,4),(-2,4))$. If a fault line is the same shape as SLRSSL up to a rotation about the origin, then there are only two possible sequences of vertex types through which it can pass: *abaaab* and *babbba*. This follows from the fact that once the first vertex type is determined, only turns in the self-avoiding walk (i.e., the L and R characters) cause the vertex type to switch. We define the weight of a fault line to be the product of the vertex types through which it passes. More generally, we define the weight of a non-backtracking walk that initially passes through a fixed vertex type to be the product of the induced vertex types according to the rule that turns toggle the current type. Formally, we let $g_a(\gamma) : \{\mathsf{S}\} \times \{\mathsf{S},\mathsf{L},\mathsf{R}\}^{n-1} \to \mathbb{R}$ denote the weight of a non-backtracking walk γ that starts by crossing a type-a vertex. We define the function $g_b(\gamma)$ similarly and note that $g_a(\mathsf{SLRSSL}) = a^4b^2$ and $g_b(\mathsf{SLRSSL}) = a^2b^4$. Last, observe that a sequence of vertex types can have many different walks in its preimage. The non-backtracking walk SRRSSR also maps to *abaaab* and *babbba* – in fact, there are $2^3 = 8$ such walks in this example since we can interchange L and R characters.

The idea of enumerating the preimages of a binary string corresponding to sequence of vertex types suggests a recursive approach for computing the sum of weighted non-backtracking walks. This naturally leads to the use of generating functions, so overload the variables x and y to also denote function arguments. For nonempty binary string $s \in \{0,1\}^n$, let $h(s)$ count the number of pairs of adjacent characters that are not equal and let $|s|$ denote the number of ones in s (e.g., if $s = 010001$ then $h(s) = 3$ and $|s| = 2$). The sum of weighted self-avoiding walks is upper bounded by the sum of weighted non-backtracking walks, so we proceed by analyzing the following function:

$$F_n(x,y) \stackrel{\text{def}}{=} \sum_{\gamma \in \{\mathsf{S}\} \times \{\mathsf{S},\mathsf{L},\mathsf{R}\}^{n-1}} g_x(\gamma) + g_y(\gamma) = \sum_{s \in \{0,1\}^n} 2^{h(s)} x^{|s|} y^{n-|s|}. \tag{3}$$

Note that $F_n(1,1) = 2 \cdot 3^{n-1}$ recovers the number of non-backtracking walks that initially cross type-a or type-b vertices. We compute a closed-form solution for $F_n(x,y)$ in the full version [13] by diagonalizing a matrix corresponding to the system of recurrence relations, which allows us to accurately capture the discrepancy between fault lines when the Boltzmann weights a and b differ.

▶ **Lemma 13.** *Let $F_n(x,y)$ be the generating function for weighted non-backtracking walks defined in (3). For any integer $n \geq 1$ and $x, y \in \mathbb{R}_{>0}$, we have*

$$F_n(x,y) \leq 3(x+y)\left(\frac{x+y+\sqrt{x^2+14xy+y^2}}{2}\right)^{n-1}.$$

We are now ready to present our Peierls argument to bound $\pi(C_{\mathrm{FL}} \cup C_{\mathrm{AFL}})$, which gives us a bound on the conductance and allows us to prove Theorem 2. First, we describe which antiferroelectric parameters cause $F_n(a/c, b/c)$ to decrease exponentially fast.

▶ **Lemma 14.** *If $(a,b,c) \in \mathbb{R}^3_{>0}$ is antiferroelectric and $3ab + ac + bc < c^2$, then we have $a + b + \sqrt{a^2 + 14ab + b^2} < 2c$.*

▶ **Lemma 15.** *If $(a,b,c) \in \mathbb{R}^3_{>0}$ is antiferroelectric and $3ab + ac + bc < c^2$, for free boundary conditions we have*

$$\pi\left(C_{\mathrm{FL}} \cup C_{\mathrm{AFL}}\right) \leq \mathrm{poly}(n)\left(\frac{a+b+\sqrt{a^2+14ab+b^2}}{2c}\right)^n.$$

Proof. For any self-avoiding walk γ and dual vertices $s, t \in L_n$ on the boundary, let $\Omega_{\gamma,s,t} \subseteq \Omega$ be the set of states containing γ as a fault line or an almost fault line such that γ starts at s and ends at t. Without loss of generality, assume that the (almost) fault line is vertical. Reversing the direction of all edges on the left side of γ defines the injective map $f_{\gamma,s,t} : \Omega_{\gamma,s,t} \to \Omega \setminus \Omega_{\gamma,s,t}$ such that if γ is a fault line of $x \in \Omega_{\gamma,s,t}$, then the weight of its image $f_{\gamma,s,t}(x)$ is amplified by $c^{|\gamma|}/g_a(\gamma)$ or $c^{|\gamma|}/g_b(\gamma)$. See Figure 5c for an example. Similarly, if γ is an almost fault line, decompose γ into subpaths γ_1 and γ_2 separated by a type-c vertex such that γ_1 starts at s and γ_2 ends at t. In this case, the weight of the images of almost fault lines is amplified by a factor of $\min(a,b)/c \cdot c^{|\gamma_1|+|\gamma_2|}/(g_\alpha(\gamma_1)g_\beta(\gamma_2))$ for some $(\alpha,\beta) \in \{a,b\}^2$. Using the fact that $f_{\gamma,s,t}$ is injective and summing over the states containing γ as a fault line and an almost fault line separately gives us

$$\pi(\Omega_{\gamma,s,t}) \leq \frac{g_a(\gamma)+g_b(\gamma)}{c^{|\gamma|}} + \frac{c}{\min(a,b)} \sum_{\gamma_1+\gamma_2=\gamma} \frac{g_a(\gamma_1)+g_b(\gamma_1)}{c^{|\gamma_1|}} \cdot \frac{g_a(\gamma_2)+g_b(\gamma_2)}{c^{|\gamma_2|}}, \tag{4}$$

where the sum is over all $\Theta(|\gamma|)$ decompositions of γ into γ_1 and γ_2.

Equipped with (4) and Lemma 13, we use a union bound over all pairs of terminals (s,t) and fault line lengths ℓ to upper bound $\pi(C_{\mathrm{FL}} \cup C_{\mathrm{AFL}})$ in terms of our generating function for weighted non-backtracking walks $F_\ell(x,y)$. Since the antiferroelectric weights satisfy $3ab + ac + bc < c^2$, it follows from Lemma 14 that

$$\begin{aligned}
\pi(C_{\mathrm{FL}} \cup C_{\mathrm{AFL}}) &\leq \sum_{(s,t)} \sum_{\ell=n}^{n^2} \left(F_\ell(a/c, b/c) + \frac{c}{\min(a,b)} \sum_{k=0}^{\ell} F_k(a/c,b/c) F_{\ell-k}(a/c,b/c) \right) \\
&\leq \sum_{(s,t)} \sum_{\ell=n}^{n^2} \mathrm{poly}(\ell) \left(\frac{a+b+\sqrt{a^2+14ab+b^2}}{2c} \right)^{\ell} \\
&\leq \mathrm{poly}(n) \left(\frac{a+b+\sqrt{a^2+14ab+b^2}}{2c} \right)^{n}.
\end{aligned}$$

Note that the convolutions in the first inequality generate all *almost* weighted non-backtracking walks. ◀

▶ **Theorem 2** (Antiferroelectric phase). *For any $(a,b,c) \in \mathbb{R}^3_{>0}$ such that $ac + bc + 3ab < c^2$, Glauber dynamics mixes exponentially slowly on Λ_n with free boundary conditions.*

Proof of Theorem 2. Let $\Omega_{\mathrm{MIDDLE}} = C_{\mathrm{FL}} \cup C_{\mathrm{AFL}}$, $\Omega_{\mathrm{LEFT}} = C_{\mathrm{R}} \setminus \Omega_{\mathrm{MIDDLE}}$, and $\Omega_{\mathrm{RIGHT}} = C_{\mathrm{G}} \setminus \Omega_{\mathrm{MIDDLE}}$. It follows from Lemma 12 that $\Omega = \Omega_{\mathrm{LEFT}} \cup \Omega_{\mathrm{MIDDLE}} \cup \Omega_{\mathrm{RIGHT}}$ is a partition with the properties that $\partial\Omega_{\mathrm{LEFT}} \subseteq \Omega_{\mathrm{MIDDLE}}$ and $\pi(\Omega_{\mathrm{LEFT}}) = \pi(\Omega_{\mathrm{RIGHT}})$. Since the partition is symmetric, Lemma 15 implies that $1/4 \leq \pi(\Omega_{\mathrm{LEFT}}) \leq 1/2$, for n sufficiently large. Therefore, we can upper bound the conductance by $\Phi^* \leq \Phi(\Omega_{\mathrm{LEFT}}) \leq 4\pi(\Omega_{\mathrm{MIDDLE}})$. Using Theorem 3 with Lemma 15 and Lemma 14 gives the desired mixing time bound. ◀

References

1 David Allison and Nicolai Reshetikhin. Numerical study of the 6-vertex model with domain wall boundary conditions. *Annales de l'institut Fourier*, 55(6):1847–1869, 2005.

2 Prateek Bhakta, Ben Cousins, Matthew Fahrbach, and Dana Randall. Approximately sampling elements with fixed rank in graded posets. In *Proceedings of the Twenty-Eighth Annual ACM-SIAM Symposium on Discrete Algorithms*, pages 1828–1838. SIAM, 2017.

3 Pavel Bleher and Vladimir Fokin. Exact solution of the six-vertex model with domain wall boundary conditions. Disordered phase. *Communications in Mathematical Physics*, 268(1):223–284, 2006.

4 Pavel Bleher and Karl Liechty. Exact solution of the six-vertex model with domain wall boundary conditions. Ferroelectric phase. *Communications in Mathematical Physics*, 286(2):777–801, 2009.

5 Pavel Bleher and Karl Liechty. Exact Solution of the Six-Vertex Model with Domain Wall Boundary Conditions: Antiferroelectric Phase. *Communications on Pure and Applied Mathematics*, 63(6):779–829, 2010.

6 N. M. Bogoliubov, A. G. Pronko, and M. B.. Zvonarev. Boundary correlation functions of the six-vertex model. *Journal of Physics A: Mathematical and General*, 35(27):5525, 2002.

7 H. J. Brascamp, H. Kunz, and F. Y. Wu. Some rigorous results for the vertex model in statistical mechanics. *Journal of Mathematical Physics*, 14(12):1927–1932, 1973.

8 Jin-Yi Cai, Zhiguo Fu, and Mingji Xia. Complexity classification of the six-vertex model. *Information and Computation*, 259:130–141, 2018.

9 Jin-Yi Cai, Tianyu Liu, and Pinyan Lu. Approximability of the Six-vertex Model. In *Proceedings of the Thirtieth Annual ACM-SIAM Symposium on Discrete Algorithms*, pages 2248–2261. SIAM, 2019.

10 Sarah Cannon and Dana Randall. Sampling on lattices with free boundary conditions using randomized extensions. In *Proceedings of the twenty-seventh annual ACM-SIAM symposium on Discrete algorithms*, pages 1952–1971. Society for Industrial and Applied Mathematics, 2016.

11 Henry Cohn, Noam Elkies, and James Propp. Local statistics for random domino tilings of the Aztec diamond. *Duke Mathematics Journal*, 85(1):117–166, October 1996. doi:10.1215/S0012-7094-96-08506-3.

12 David Durfee, Matthew Fahrbach, Yu Gao, and Tao Xiao. Nearly tight bounds for sandpile transience on the grid. In *Proceedings of the Twenty-Ninth Annual ACM-SIAM Symposium on Discrete Algorithms*, pages 605–624. SIAM, 2018.

13 Matthew Fahrbach and Dana Randall. Slow Mixing of Glauber Dynamics for the Six-Vertex Model in the Ferroelectric and Antiferroelectric Phases. *arXiv preprint*, 2019. arXiv:1904.01495.

14 Patrik L. Ferrari and Herbert Spohn. Domino tilings and the six-vertex model at its free-fermion point. *Journal of Physics A: Mathematical and General*, 39(33):10297, 2006.

15 J. Gillis. Correlated random walk. *Mathematical Proceedings of the Cambridge Philosophical Society*, 51(4):639–651, 1955.

16 Leslie Ann Goldberg, Russell Martin, and Mike Paterson. Random sampling of 3-colorings in $\mathbb{Z}^2$. *Random Structures & Algorithms*, 24(3):279–302, 2004.

17 A. J. Guttmann and A. R. Conway. Square lattice self-avoiding walks and polygons. *Annals of Combinatorics*, 5(3-4):319–345, 2001.

18 J. W. Hanneken and D. R. Franceschetti. Exact distribution function for discrete time correlated random walks in one dimension. *The Journal of Chemical Physics*, 109(16):6533–6539, 1998.

19 Lingxiao Huang, Pinyan Lu, and Chihao Zhang. Canonical paths for MCMC: From art to science. In *Proceedings of the Twenty-Seventh Annual ACM-SIAM Symposium on Discrete Algorithms*, pages 514–527. Society for Industrial and Applied Mathematics, 2016.

20 Anatoli G Izergin, David A Coker, and Vladimir E Korepin. Determinant formula for the six-vertex model. *Journal of Physics A: Mathematical and General*, 25(16):4315, 1992.

21 David Keating and Ananth Sridhar. Random tilings with the GPU. *Journal of Mathematical Physics*, 59(9):091420, 2018.

22 Vladimir Korepin and Paul Zinn-Justin. Thermodynamic limit of the six-vertex model with domain wall boundary conditions. *Journal of Physics A: Mathematical and General*, 33(40):7053, 2000.

23 Greg Kuperberg. Another proof of the alternative-sign matrix conjecture. *International Mathematics Research Notices*, 1996(3):139–150, 1996.

24 David A. Levin, Yuval Peres, and Elizabeth L. Wilmer. *Markov Chains and Mixing Times*, volume 107. American Mathematical Society, 2017.

25 Elliott H Lieb. Exact solution of the problem of the entropy of two-dimensional ice. *Physical Review Letters*, 18(17):692, 1967.

26 Elliott H Lieb. Exact Solution of the Two-Dimensional Slater KDP Model of a Ferroelectric. *Physical Review Letters*, 19(3):108, 1967.

27 Elliott H Lieb. Residual Entropy of Square Ice. *Physical Review*, 162(1):162, 1967.

28 Tianyu Liu. Torpid Mixing of Markov Chains for the Six-vertex Model on $\mathbb{Z}^2$. In *Approximation, Randomization, and Combinatorial Optimization. Algorithms and Techniques* (APPROX/RANDOM). Schloss Dagstuhl-Leibniz-Zentrum fuer Informatik, 2018.

29 Michael Luby, Dana Randall, and Alistair Sinclair. Markov chain algorithms for planar lattice structures. *SIAM Journal on Computing*, 31(1):167–192, 2001.

30 Ivar Lyberg, Vladimir Korepin, G. A. P. Ribeiro, and Jacopo Viti. Phase separation in the six-vertex model with a variety of boundary conditions. *Journal of Mathematical Physics*, 59(5):053301, 2018.

31 Ivar Lyberg, Vladimir Korepin, and Jacopo Viti. The density profile of the six vertex model with domain wall boundary conditions. *Journal of Statistical Mechanics: Theory and Experiment*, 2017(5):053103, 2017.

32 Colin McQuillan. Approximating holant problems by winding. *arXiv preprint*, 2013. `arXiv:1301.2880`.

33 Linus Pauling. The structure and entropy of ice and of other crystals with some randomness of atomic arrangement. *Journal of the American Chemical Society*, 57(12):2680–2684, 1935.

34 Yuval Peres and Perla Sousi. Mixing times are hitting times of large sets. *Journal of Theoretical Probability*, 28(2):488–519, 2015.

35 Dana Randall. Slow mixing of Glauber dynamics via topological obstructions. In *Proceedings of the Seventeenth Annual ACM-SIAM Symposium on Discrete Algorithms*, pages 870–879. Society for Industrial and Applied Mathematics, 2006.

36 Dana Randall and Prasad Tetali. Analyzing Glauber dynamics by comparison of Markov chains. *Journal of Mathematical Physics*, 41(3):1598–1615, 2000.

37 Eric Renshaw and Robin Henderson. The correlated random walk. *Journal of Applied Probability*, 18(2):403–414, 1981.

38 Bill Sutherland. Exact solution of a two-dimensional model for hydrogen-bonded crystals. *Physical Review Letters*, 19(3):103, 1967.

39 David Bruce Wilson. Mixing times of lozenge tiling and card shuffling Markov chains. *The Annals of Applied Probability*, 14(1):274–325, 2004.

40 C. P. Yang. Exact solution of a model of two-dimensional ferroelectrics in an arbitrary external electric field. *Physical Review Letters*, 19(10):586, 1967.

41 Doron Zeilberger. Proof of the alternating sign matrix conjecture. *Electronic Journal of Combinatorics*, 3(2):R13, 1996.

A Tail Behavior of Correlated Random Walks

In this section we prove Lemma 8, which gives an exponentially small upper bound for the tail of a correlated random walk as a function of its momentum parameter μ. Our proof builds off of the PDF for the position of a correlated random walk given as Lemma 4, which is combinatorial in nature and not readily amenable for tail inequalities. Specifically, the probability $\Pr(S_{2n} = 2m)$ is a sum of marginals conditioned on the number of turns that the walk makes [37].

There are two main ideas in our approach to develop a more useful bound for the position of a correlated random walk $\Pr(S_{2n} = 2m)$. First, we construct a smooth function that upper bounds the marginals as a function of x (a continuation of the number of turns in the walk k), and then we determine its maximum value. Next we show that the log of the maximum value is asymptotically equivalent to $m^2/(\mu n)$ for $m = o(n)$, which gives us desirable bounds

for sufficiently large values of n. We point out that this analysis illustrates precisely how correlated random walks generalize simple symmetric random walks and how the momentum parameter μ controls the exponential decay.

A.1 Upper Bounding the Marginal Probabilities

We start by using Stirling's approximation to construct a smooth function that upper bounds the marginal terms in the sum of the PDF for correlated random walks. For $x \in (0, n-m)$, let

$$f(x) \stackrel{\text{def}}{=} \begin{cases} 1 & \text{if } x = 0, \\ \frac{(n+m)^{n+m}}{x^x (n+m-x)^{n+m-x}} \cdot \frac{(n-m)^{n-m}}{x^x (n-m-x)^{n-m-x}} \cdot \mu^{-2x} & \text{if } x \in (0, n-m), \\ \mu^{-2(n-m)} & \text{if } x = n-m. \end{cases} \tag{5}$$

It can easily be checked that $f(x)$ is continuous on all of $[0, n-m]$ since $\lim_{x \to 0} x^x = 1$.

▶ **Lemma 16.** *For any integer $m \geq 0$, a correlated random walk satisfies*

$$\Pr(S_{2n} = 2m) \leq \text{poly}(n) \sum_{k=0}^{n-m} \left(\frac{\mu}{1+\mu}\right)^{2n} f(k).$$

Proof. Consider the probability density function for $\Pr(S_{2n} = 2m)$ in Lemma 4. If $2m = 2n$ the claim is clearly true, so we focus on the other case. We start by bounding the rightmost polynomial term in the sum. For all $n \geq 1$, we have $n(1-p) + k(2p-1) \leq 2nk$. Next, we reparameterize the marginals in terms of μ, where $p = \mu/(1+\mu)$, and use a more convenient upper bound for the binomial coefficients. Observe that

$$\begin{aligned} \Pr(S_{2n} = 2m) &\leq 2n \sum_{k=1}^{n-m} \binom{n+m-1}{k-1} \binom{n-m-1}{k-1} \left(\frac{1}{1+\mu}\right)^{2k-1} \left(\frac{\mu}{1+\mu}\right)^{2n-1-2k} \\ &\leq \text{poly}(n) \sum_{k=0}^{n-m} \binom{n+m}{k} \binom{n-m}{k} \left(\frac{\mu}{1+\mu}\right)^{2n} \mu^{-2k}. \end{aligned}$$

Stirling's approximation states that for all $n \geq 1$ we have $e(n/e)^n \leq n! \leq en(n/e)^n$, so we can bound the products of binomial coefficients up to a polynomial factor by

$$\begin{aligned} \binom{n+m}{k} \binom{n-m}{k} &\leq \text{poly}(n) \cdot \frac{\left(\frac{n+m}{e}\right)^{n+m}}{\left(\frac{k}{e}\right)^k \left(\frac{n+m-k}{e}\right)^{n+m-k}} \cdot \frac{\left(\frac{n-m}{e}\right)^{n-m}}{\left(\frac{k}{e}\right)^k \left(\frac{n-m-k}{e}\right)^{n-m-k}} \\ &= \text{poly}(n) \cdot \frac{(n+m)^{n+m}}{k^k (n+m-k)^{n+m-k}} \cdot \frac{(n-m)^{n-m}}{k^k (n-m-k)^{n-m-k}}. \end{aligned}$$

The proof follows the definition of $f(x)$ given in (5). ◀

There are polynomially-many marginal terms in the sum of the PDF, so if the maximum term is exponentially small, then the total probability is exponentially small. Since the marginal terms are bounded above by an expression involving $f(x)$, we can proceed by maximizing $f(x)$ on its support.

▶ **Lemma 17.** *The function $f(x)$ is maximized at the critical point*

$$x^* = \begin{cases} \frac{n^2 - m^2}{2n} & \text{if } \mu = 1, \\ \frac{n}{1-\mu^2} \left(1 - \sqrt{\mu^2 + (1-\mu^2)\frac{m^2}{n^2}}\right) & \text{otherwise.} \end{cases}$$

Proof. We start by showing that $f(x)$ is log-concave on $(0, n-m)$, which implies that it is unimodal. It follows that a local maximum of $f(x)$ is a global maximum. Since n and k are fixed as constants and because the numerator is positive, it is sufficient to show that

$$\begin{aligned} g(x) &= -\log\big(x^x(n+m-x)^{n+m-x} \cdot x^x(n-m-x)^{n-m-x} \cdot \mu^{2x}\big) \\ &= -(2x\log(\mu x) + (n+m-x)\log(n+m-x) + (n-m-x)\log(n-m-x)) \end{aligned}$$

is concave. Observe that the first derivative of $g(x)$ is

$$\begin{aligned} g'(x) &= -2(1+\log(\mu x)) + (1+\log(n+m-x)) + (1+\log(n-m-x)) \\ &= -2\log(\mu x) + \log(n+m-x) + \log(n-m-x), \end{aligned}$$

and the second derivative is

$$g''(x) = -\frac{2}{x} - \frac{1}{n+m-x} - \frac{1}{n-m-x}.$$

Because $g''(x) < 0$ on $(0, n-m)$, the function $f(x)$ is log-concave and hence unimodal.

To identify the critical points of $f(x)$, it suffices to determine where $g'(x) = 0$ since $\log x$ is increasing. Using the previous expression for $g'(x)$, it follows that

$$g'(x) = \log\left[\frac{(n-x)^2 - m^2}{\mu^2 x^2}\right]. \tag{6}$$

Therefore, the critical points are the solutions of $(n-x)^2 - m^2 = \mu^2 x^2$, so we have

$$x^* = \begin{cases} \frac{n^2-m^2}{2n} & \text{if } \mu = 1, \\ \frac{n - \sqrt{n^2 - (1-\mu^2)(n^2-m^2)}}{1-\mu^2} & \text{otherwise.} \end{cases}$$

It remains and suffices to show that x^* is a local maximum since $f(x)$ is unimodal. Observing that $\frac{\partial}{\partial x}\log f(x) = g'(x)$ and differentiating $f(x) = \exp(\log f(x))$ using the chain rule, the definition of x^* gives

$$f''(x^*) = e^{\log f(x^*)}\Big[g''(x^*) + g'(x^*)^2\Big] = f(x^*)g''(x^*).$$

We know $f(x^*) > 0$, so $f''(x^*)$ has the same sign as $g''(x^*) < 0$. Therefore, x^* is a local maximum of $f(x)$. Using the continuity of $f(x)$ on $[0, n-m]$ and log-concavity, $f(x^*)$ is a global maximum. ◀

A.2 Asymptotic Behavior of the Maximum Log Marginal

Now that we have a formula for x^*, and hence an expression for $f(x^*)$, we want to show that

$$\left(\frac{\mu}{1+\mu}\right)^{2n} f(x^*) \le e^{-n^c},$$

for some constant $c > 0$. Because there are polynomially-many marginals in the sum, this leads to an exponentially small upper bound for $\Pr(S_{2n} = 2m)$. Define the *maximum log marginal* to be

$$h(n) \stackrel{\text{def}}{=} -\log\left[\left(\frac{\mu}{1+\mu}\right)^{2n} f(x^*)\right]. \tag{7}$$

Equivalently, we show that $h(n) \ge n^c$ for sufficiently large n using asymptotic equivalences.

▶ **Lemma 18.** *The maximum log marginal $h(n)$ can be symmetrically expressed as*

$$h(n) = (n+m)\log\left[\left(\frac{1+\mu}{\mu}\right)\left(1-\frac{x^*}{n+m}\right)\right] + (n-m)\log\left[\left(\frac{1+\mu}{\mu}\right)\left(1-\frac{x^*}{n-m}\right)\right].$$

Proof. Grouping the terms of $h(n)$ by factors of n, m and x^* gives

$$n\log\left[\left(\frac{1+\mu}{\mu}\right)^2\frac{(n-x^*)^2-m^2}{(n+m)(n-m)}\right] + m\log\left[\frac{(n-m)(n+m-x^*)}{(n+m)(n-m-x^*)}\right] + x^*\log\left[\frac{(\mu x^*)^2}{(n-x^*)^2-m^2}\right].$$

Using (6), observe that the last term is

$$x^*\log\left[\frac{(\mu x^*)^2}{(n-x^*)^2-m^2}\right] = -x^* g'(x^*) = 0.$$

The proof follows by grouping the terms of the desired expression by factors of n and m. ◀

The following lemma is the crux of our argument, as it presents an asymptotic equality for the maximum log marginal in the PDF for correlated random walks. We remark that we attempted to bound this quantity directly using Taylor expansions instead of an asymptotic equivalence, and while this seems possible, the expressions are unruly. Our asymptotic equivalence demonstrates that second derivative information is needed, which makes the earlier approach even more unmanageable.

▶ **Lemma 19.** *For $\mu > 0$ and $m = o(n)$, the maximum log marginal satisfies $h(n) \sim m^2/(\mu n)$.*

Proof. The proof is by case analysis for μ. In both cases we analyze $h(n)$ as expressed in Lemma 18, consider a change of variables, and use L'Hospital's rule twice. In the first case, we assume $\mu = 1$. The value of x^* in Lemma 17 gives us

$$1-\frac{x^*}{n+m} = \frac{2n(n+m)-\left(n^2-m^2\right)}{2n(n+m)} = \frac{n+m}{2n}$$
$$1-\frac{x^*}{n-m} = \frac{2n(n-m)-\left(n^2-m^2\right)}{2n(n-m)} = \frac{n-m}{2n}.$$

It follows that $h(n)$ can be simplified as

$$h(n) = n\log\left[\left(\frac{1+\mu}{\mu}\right)^2\left(\frac{n^2-m^2}{4n^2}\right)\right] + m\log\left(\frac{n+m}{n-m}\right) = n\log\left(1-\frac{m^2}{n^2}\right) + m\log\left(1+\frac{2m}{n-m}\right).$$

To show $h(n) \sim m^2/n$, by the definition of asymptotic equivalence we need to prove that

$$\lim_{n\to\infty}\frac{n\log\left(1-\frac{m^2}{n^2}\right)+m\log\left(1+\frac{2m}{n-m}\right)}{\frac{m^2}{n}} = 1.$$

Make the change of variables $y = m/n$. Since $m = o(n)$, this is equivalent to showing

$$\lim_{y\to 0}\frac{\log\left(1-y^2\right)+y\log\left(1+\frac{2y}{1-y}\right)}{y^2} = 1.$$

Using L'Hospital's rule twice with the derivatives

$$\frac{\partial}{\partial y}\left[\log\left(1-y^2\right)+y\log\left(1+\frac{2y}{1-y}\right)\right] = \log\left(-\frac{y+1}{y-1}\right)$$
$$\frac{\partial^2}{\partial y^2}\left[\log\left(1-y^2\right)+y\log\left(1+\frac{2y}{1-y}\right)\right] = \frac{2}{1-y^2},$$

it follows that

$$\lim_{y\to 0}\frac{\log(1-y^2)+y\log\left(1+\frac{2y}{1-y}\right)}{y^2}=\lim_{y\to 0}\frac{\log\left(-\frac{y+1}{y-1}\right)}{2y}=\lim_{y\to 0}\frac{\frac{2}{1-y^2}}{2}=1.$$

This completes the proof for $\mu = 1$.

The case when $\mu \neq 1$ is analogous but messier. Making the same change of variables $y = m/n$, it is equivalent to show that

$$\begin{aligned}&(1+y)\log\left[\left(\frac{1+\mu}{\mu}\right)\left(1-\frac{1}{1-\mu^2}\cdot\frac{1}{1+y}\cdot\left(1-\sqrt{\mu^2+(1-\mu^2)y^2}\right)\right)\right]\\&+(1-y)\log\left[\left(\frac{1+\mu}{\mu}\right)\left(1-\frac{1}{1-\mu^2}\cdot\frac{1}{1-y}\cdot\left(1-\sqrt{\mu^2+(1-\mu^2)y^2}\right)\right)\right]\sim\mu^{-1}y^2,\end{aligned}\quad(8)$$

because the value of x^* for $\mu \neq 1$ in Lemma 17 gives us

$$1-\frac{x^*}{n+m}=1-\frac{1}{n+m}\cdot\frac{n}{1-\mu^2}\cdot\left(1-\sqrt{\mu^2+(1-\mu^2)\frac{m^2}{n^2}}\right).$$

Denoting the left-hand side of (8) by $g(y)$, one can verify the first two derivatives of $g(y)$ are

$$\begin{aligned}g'(y)&=\log\left(\frac{\mu^2-\sqrt{\mu^2-\mu^2y^2+y^2}+\left(\mu^2-1\right)y}{(\mu-1)\mu(y+1)}\right)-\log\left(\frac{-\mu^2+\sqrt{\mu^2-\mu^2y^2+y^2}+\left(\mu^2-1\right)y}{(\mu-1)\mu(y-1)}\right)\\g''(y)&=\frac{2}{(1+y)(1-y)\sqrt{y^2-\mu^2(y^2-1)}}.\end{aligned}$$

Observing that $g(0) = g'(0) = 0$ due to cancellations and using L'Hospital's rule twice,

$$\lim_{y\to 0}\frac{g(y)}{\mu^{-1}y^2}=\lim_{y\to 0}\frac{g'(y)}{2\mu^{-1}y}=\lim_{y\to 0}\frac{2}{(1+y)(1-y)\sqrt{y^2-\mu^2(y^2-1)}}\cdot\frac{\mu}{2}=1.$$

This completes the proof for all cases of μ. ◀

▶ **Lemma 8.** *Let $\mu, \varepsilon > 0$ and $m = o(n)$. For n sufficiently large, a correlated random walk satisfies* $\Pr(S_{2n} = 2m) \leq e^{-(1-\varepsilon)\frac{m^2}{\mu n}}$.

Proof. For n sufficiently large, the asymptotic equality for $h(n)$ in Lemma 19 gives us

$$h(n)\geq\left(1-\frac{\varepsilon}{2}\right)\frac{m^2}{\mu n}.$$

It follows from our construction of $f(x)$ and the definition of the maximum log marginal that

$$\begin{aligned}\Pr(S_{2n}=2m)&\leq\operatorname{poly}(n)\cdot\left(\frac{\mu}{1+\mu}\right)^{2n}f(x^*)\\&=\operatorname{poly}(n)\cdot e^{-h(n)}\\&\leq\operatorname{poly}(n)\cdot e^{-\left(1-\frac{\varepsilon}{2}\right)\frac{m^2}{\mu n}}\\&\leq e^{-(1-\varepsilon)\frac{m^2}{\mu n}},\end{aligned}$$

as desired. ◀